



Structural hierarchies define toughness and defect-tolerance despite simple and mechanically inferior brittle building blocks

Dipanjan Sen^{1,2} & Markus J. Buehler¹

¹Laboratory for Atomistic and Molecular Mechanics, Department of Civil and Environmental Engineering, 77 Massachusetts Ave. Room 1-235A&B, Cambridge, MA, USA, ²Department of Materials Science and Engineering, Massachusetts Institute of Technology 77 Mass. Ave., Cambridge, MA 02139, USA.

Received
14 February 2011

Accepted
17 May 2011

Published
13 July 2011

Correspondence and requests for materials should be addressed to M.J.B. (mbuehler@MIT.EDU)

SUBJECT AREAS:
BIOMATERIALS
MATERIALS
MECHANICAL PROPERTIES
MODELLING AND THEORY

Mineralized biological materials such as bone, sea sponges or diatoms provide load-bearing and armor functions and universally feature structural hierarchies from nano to macro. Here we report a systematic investigation of the effect of hierarchical structures on toughness and defect-tolerance based on a single and mechanically inferior brittle base material, silica, using a bottom-up approach rooted in atomistic modeling. Our analysis reveals drastic changes in the material crack-propagation resistance (R-curve) solely due to the introduction of hierarchical structures that also result in a vastly increased toughness and defect-tolerance, enabling stable crack propagation over an extensive range of crack sizes. Over a range of up to four hierarchy levels, we find an exponential increase in the defect-tolerance approaching hundred micrometers without introducing additional mechanisms or materials. This presents a significant departure from the defect-tolerance of the base material, silica, which is brittle and highly sensitive even to extremely small nanometer-scale defects.

This work addresses a fundamental question — is it possible, and if yes, how, to create materials with enhanced mechanical properties based on a single and mechanically inferior material, solely by using geometry as a design parameter? Many biological materials with a structural purpose, such as bone, nacre, sea sponge exoskeletons, diatoms and spider silk^{1–9}, showcase the use of structurally inferior building blocks, arranged in multiple levels of hierarchical structure. These materials are used for load-bearing, skeletal support or armor protection applications and require excellent mechanical properties, including great robustness against catastrophic material failure. In particular, high toughness—quantifying the capacity of a material to dissipate energy under large loading—is a vital material property for these biological applications. Experimentally, the fracture behavior of materials such as bone and nacre have been shown to be intimately linked across multiple structural length scales^{10,11}, with mechanisms at several different hierarchy levels participating in the overall behavior^{12–14}. A fundamental question, however, remains, whether or not specific base materials or mechanisms (e.g.: reinforcement materials, an organic phase, specific interfaces or interfacial effects, grain boundaries, etc.) are needed in order to achieve enhanced mechanical properties at larger scales. Since the impact of hierarchical structures alone on toughness cannot easily be quantitatively compared to other toughness improvement techniques, the understanding and use of hierarchies as a sole design variable in the bottom-up design of materials remains limited.

A thorough understanding of the mechanical properties of hierarchical materials can be achieved through the development of models that appropriately reflect their structural and mechanistic nature from the bottom up. A pioneering theoretical approach in addressing this issue has been the study of self-similar hierarchical assemblies with some assumptions about similarity in failure mechanisms at each hierarchy level, using continuum mechanics^{15–18}. These continuum-level models can predict the strength, stiffness and toughness scaling with the number of hierarchy levels and have been applied to several cases. Applications included a self-similar hierarchical assembly of the bone nanostructure¹⁶ and gecko adhesion^{19,20}. Self-similarity in geometric design, however, is not always observed in biological materials, and in particular in bone, nacre, sea sponge exoskeletons, diatom algae and other case^{3,4,21,22}, the structural arrangement at each hierarchy level is quite different. Another approach has been to take into account explicit probabilistic modes of failure pathways in several levels of



hierarchy, under the assumption of certain unit failure events (e.g., failure of unit hydrogen bond clusters in hierarchical alpha-helix structures)^{23,24}. Some qualitative models have been derived to identify design similarities in the hierarchical structures of biological materials that may offer the key to improvements of properties^{25–27}. Limitations to existing models remain with respect to their ability to provide a complete description of the mechanism of failure for example via crack propagation.

Here we use a bottom-up approach to systematically examine the effects of hierarchical structures on fracture toughness by investigating how crack propagation is modified solely through the presence of hierarchical structures and without adding additional materials or mechanisms. We specifically consider that, from a fracture mechanics^{28–30} point of view, a single major crack propagates through the material and leads to failure and that therefore this one crack interacts with all levels of hierarchy. We also examine the defect-tolerance length scale, which measures the sensitivity of fracture strength to the presence and size of a crack; where a higher defect-tolerance implies a lower sensitivity to crack size, *i.e.*, a large change in the size of a crack in the material leads only to a relatively small change in the fracture strength.

We use silica as a single base material for constructing various hierarchical structures to represent a set of model materials that are used to carry out a series of computational experiments. The choice of silica as a base material is inspired by the dominant material found in many mineralized organisms such as diatoms and deep sea sponges^{3,31}, which showcase the use of a predominantly silica-based structure (with up to 97–99% silica content) that result in protective exoskeletons that perform much better than the base material alone; which is stiff but very fragile and thus mechanically inferior.

Previous work based on first principles based reactive modeling has demonstrated that nanoporous silica as found in diatom algae, for example, is mechanically deformable and “ductile” (tough), but very soft^{32,33} (Fig. 1a–b). It was demonstrated³⁴ that the geometry of this structure, with nanoscale silica struts confined to a few nanometer cross-section, is critical in providing the highly deformable material behavior; which also agrees qualitatively with size-dependent experimental results in silicon³⁵. The earlier atomistic modeling showed that each strut is in a flaw-tolerant state that is characterized by a largely homogeneous stress state¹³, facilitating a ductile-like behavior of silica. Even though the individual struts reach very high strengths under this geometric confinement, the overall strength of

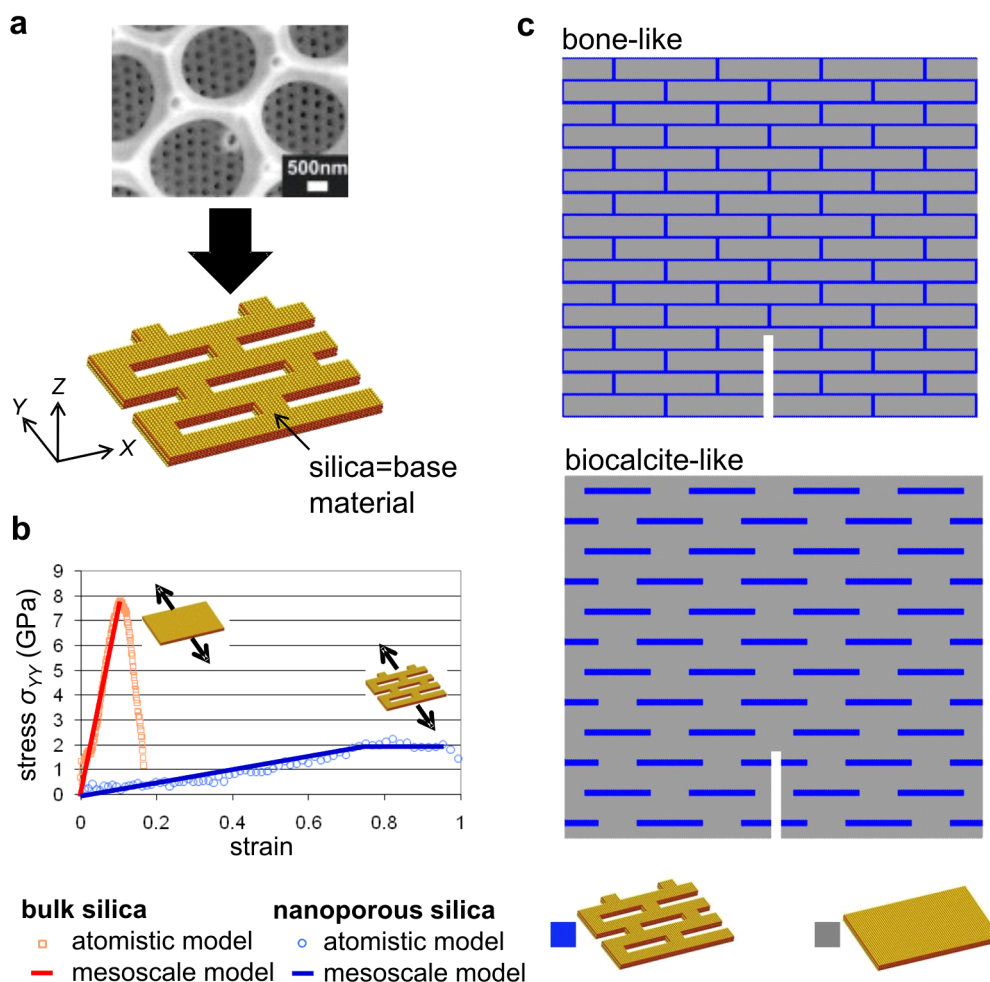


Figure 1 | Structure and properties of nanoporous silica inspired from the nanostructure of diatom algae, and two commonly occurring periodic motifs chosen for the nanoporous silica/bulk silica composites. **a**, Scanning Electron Microscope (SEM) image of a diatom nanostructure (image reprinted with permission from Ref. 49) and full-atomistic model of α -quartz nanoporous silica, stress-strain response obtained from atomistic simulations of tensile loading of the nanoporous silica and bulk silica. **b**, Mesoscale model stress-strain response. The base material for both structures is silica and identical for both structures but the different organization leads to a drastically changed mechanical response (the stress-strain data shown is averaged over a representative cell in each case). **c**, Representation of two biological structures, *bone-like* and *biocalcite-like*. The upper structure (*bone-like*) represents one in which the soft/tough nanoporous silica material is the matrix phase in which hard/brittle bulk silica platelets are dispersed. In the lower structure (*biocalcite-like*) the hard/brittle bulk silica material serves as the matrix material in which soft/tough nanoporous silica platelets are dispersed. These structures mimic those seen in bone and nacre biological calcite single crystals, respectively^{37,38}.



the nanoporous material (averaged over a representative element of the porous material) is smaller due to the relatively low volume fraction of silica (Fig. 1b).

The natural nanoporous geometry found at the lowest level of the structural hierarchy, and the corresponding nanoporous α -quartz silica structure inspired from this geometry, are shown in Fig. 1a. The soft, deformable and “ductile” (tough) nanoporous silica is combined with stiff and brittle bulk silica, forming two material phases as fundamental building blocks at the next level of hierarchy that allows us to use a *single material* as the fundamental building block, but organized hierarchically in different geometries. Many biological materials contain not only mineral phases but a combination of mineral and organic (e.g.: protein) phase. In the spirit of using a single material in constructing hierarchical materials, the protein phase found in biological materials such as bone, which is soft, extensible and “ductile” (tough), is replaced by nanoporous silica in our structures. The mineral constituent, which is hard and brittle, is replaced by bulk silica. No interfacial effects between any two phases are considered, reflecting that all structures are composed of a perfectly bonded single material as the fundamental building block.

To enable us to access the scales associated with such hierarchical materials (approaching hundred micrometers) we use an *in silico* multiscale approach based on a mesoscopic model that describes the material as a collection of particles connected by nonlinear springs (details of the atomistically-informed mesoscale method are presented in the Methods section, the Supplementary Information material, as well as in³⁶). We emphasize that the model

used here is designed by our desire to derive generic insight into the mechanical properties and deformation mechanisms valid for a broader class of biological materials, and not for one specific material. While such a simple model formulation does not allow us to derive quantitative properties of specific types of biological materials, it enables us to understand generic mechanisms that control the failure behavior of hierarchical materials and to carry out a systematic comparison of different structural designs.

Results

Two-hierarchy level structures. We first consider regularly distributed composite structures with two levels of hierarchy. For a particle-reinforced composite, two distinct design schemes are possible. One in which the soft material is the matrix, and another one where the soft material makes up the reinforcement particles. Both cases are observed in biological materials, and in order to investigate both we choose two representative systems. In the first one (“*bone-like*”) the soft, deformable and “ductile” (tough) material is the continuous phase, with the hard and brittle material dispersed in platelet form within the matrix, mimicking the periodic arrangement observed in several hierarchy levels in bone and nacre¹. The second case (“*biocalcite-like*”) is where the hard and brittle constituent is the continuous phase, with regions of soft, deformable and “ductile” (tough) material embedded within the hard matrix. These structures are found in biological crystals where protein material is encapsulated in a hard crystal, such as biological calcite single crystals^{37,38}. The use of a periodic distribution of one material in another not only allows us to

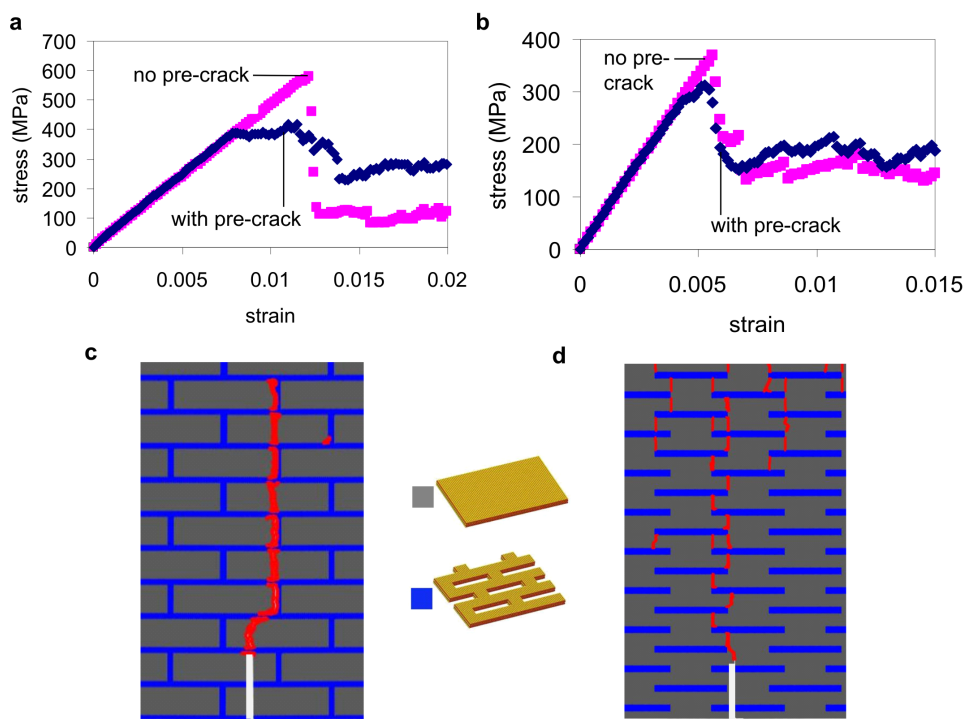


Figure 2 | Characteristic stress–strain curves with and without a crack for two geometries and associated crack propagation paths (initial crack: white line, crack path: red line). a, *Bone-like* composite structures, with and without presence of a pre-crack (pre-crack length 5.4 μm). The fracture strength changes drastically upon the introduction of a crack. b, Stress–strain curves for a *biocalcite-like* composite structure, with and without presence of a pre-crack (pre-crack length 6.96 μm). The sensitivity to fracture strength is much smaller than for the *bone-like* composite, although the magnitude of the fracture strength is lower. c and d, Crack pathways (marked in red) for *bone-like* and *biocalcite-like* hierarchical structures in the presence of a pre-crack. c, The image shows that for *bone-like* structures, the pre-crack propagates through the sample, but the structure is toughened by the platelets bridging the wake of the crack as it propagates. d, For small crack sizes failure in the *biocalcite-like* structure propagates through the nucleation of several micro-cracks at nanoporous silica/bulk-silica interfaces located far from the original crack tip. The fracture strength is reached when several of these micro-cracks link up along with the pre-crack to create a complete failure path through the sample. These results show that different crack propagation paths in the two structures lead to different defect-tolerance responses.



capture actual design morphologies observed in biological structures, but also removes stochastic elements of the dependence of mechanical properties on random morphologies. The volume fraction of the stiff silica phase is kept at a high value and constant at 80% for all structures under consideration; where this high value is important to maintain a high modulus.

Both composite structures considered in the analysis of two-hierarchy structures are shown in Fig. 1c. For the *bone-like* arrangement, the platelets of bulk silica have a rectangular shaped cross-section and $8.4\ \mu\text{m}$ by $2.4\ \mu\text{m}$ in size in the *X-Y* plane, and $100\ \text{nm}$ in the out-of-plane direction. They are arranged in a staggered fashion, with an overlap equal to half their length across subsequent layers. The overall size of the structure considered here is $27\ \mu\text{m}$ by $70\ \mu\text{m}$ and $100\ \text{nm}$ out-of-plane. For the *biocalcite-like* arrangement, the soft nanoporous silica is embedded as rectangular inclusions with a cross-section size of $8.7\ \mu\text{m}$ by $0.7\ \mu\text{m}$ in size in the *X-Y* plane, and $100\ \text{nm}$ in the out-of-plane *Z*-direction. Next we create sharp edge cracks in all structures and load them under quasi-static tensile mode I loading. Initial crack sizes considered range from ≈ 5 to $20\ \mu\text{m}$, and crack initiation is identified by the advance of the crack front at a particular applied strain. Figure 2a shows representative stress-strain responses for structures with *bone-like* and *biocalcite-like* morphologies, with and without the presence of the edge crack. The data shows that both structures feature a drop in fracture stress under the presence of a crack. The *bone-like* structure has a higher fracture stress but shows a larger drop in strength when a crack is introduced, whereas the *biocalcite-like* structure has smaller fracture strength, but also a lower sensitivity to the presence of a crack. Thus the *biocalcite-like* structure shows a higher defect-tolerance at the cost of a lower fracture strength.

Taking a closer look at the fracture mechanics and crack propagation behavior in both structures, Fig. 2b provides an indication as to why the *biocalcite-like* structure feature a higher defect-tolerance. For small crack sizes, failure in these materials propagates through the nucleation of several micro-cracks at nano-porous silica/bulk-silica interfaces located far from the original crack tip. This makes the failure morphology appear quite similar in the presence of smaller cracks and in the absence of any, and provides comparable fracture strength values. On the other hand, for the *bone-like* structures, the pre-crack always propagates as an individual crack, but toughening occurs by platelets bridging the wake of the crack as it propagates. This analysis shows that a change of the structural arrangements of the material has the potential to direct a significant alteration of the fracture properties, despite the same single material constituent and identical volume fraction in both cases.

Extension to three- and four-hierarchy level structures. To assess the effect of additional hierarchy levels on the mechanical properties, the two-hierarchy structures discussed in the previous section are now extended to feature additional levels of hierarchy. Both self-similar geometries, in the vein of earlier studies¹⁶, and dissimilar geometries are considered (see insets in Fig. 3). Even though self-similar (fractal) geometries are not found widely in biological materials, they have been used in the literature to build theoretical and computational models of hierarchical structures and are therefore also included here. Dissimilar geometries are considered as representative cases of how the geometry at different hierarchy levels in bone, diatoms and other biological materials can be quite different from one another. The self-similar geometry uses a replica of the *bone-like* arrangement at different scales (Fig. 3b inset). The

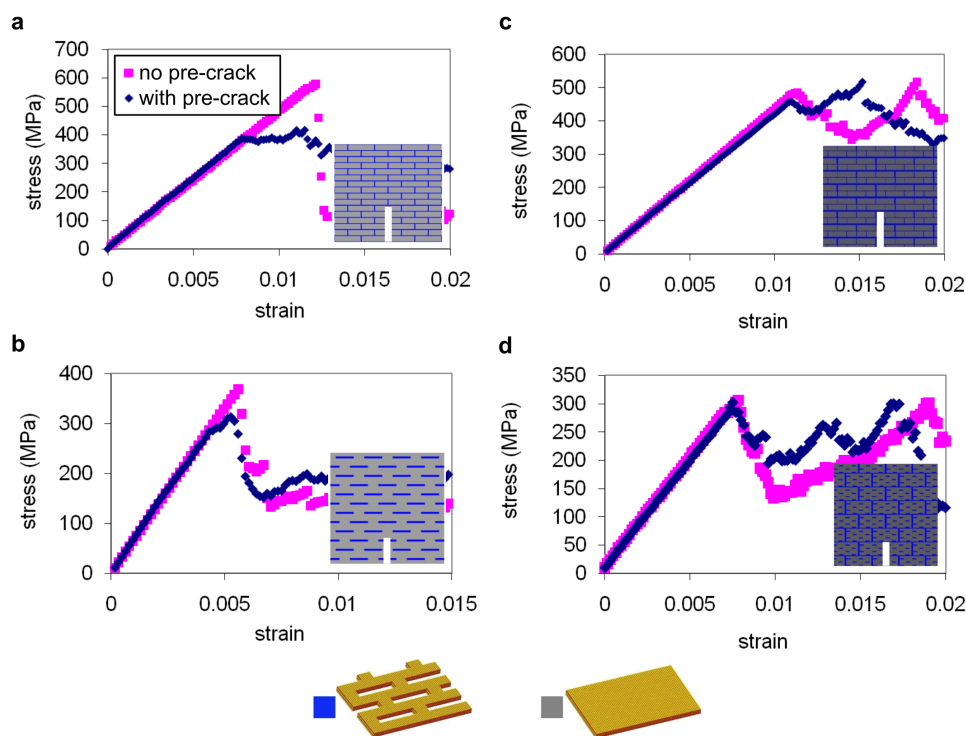


Figure 3 | Comparison of the stress-strain response of two-hierarchy (a, b) and three-hierarchy (c, d) materials, considering both self-similar (a, c) and dissimilar (c, d) designs. a, Stress-strain curves for the two-hierarchy *bone-like* composite structures, with and without presence of a pre-crack (pre-crack length $5.8\ \mu\text{m}$). b, Stress-strain curves for two-hierarchy *biocalcite-like* composite structures, with and without presence of a pre-crack (pre-crack length $6.96\ \mu\text{m}$). c, Three-hierarchy self-similar structure made of *bone-like* composite structure at both the second and third levels, with and without presence of a pre-crack (pre-crack length $4.8\ \mu\text{m}$). The data shows that the sensitivity of fracture strength vs. crack size is much smaller for the three-hierarchy material. d, Three-hierarchy dissimilar structure made of *biocalcite-like* composite structure at the second level and *bone-like* at the third level, with and without presence of a pre-crack (pre-crack length $5.8\ \mu\text{m}$). Similar as for the case presented in panel c, the sensitivity of fracture strength vs. crack size is smaller for the three-hierarchy material than for the two-hierarchy case.



platelets size at the second level of hierarchy is $5.95 \mu\text{m}$ by $1.16 \mu\text{m}$ in cross-section, while at the third level it is $12.7 \mu\text{m}$ by $5.4 \mu\text{m}$. The overall sample size is $54 \mu\text{m}$ by $70 \mu\text{m}$ in the X - Y plane, and 100 nm in the out-of-plane Z -direction. The dissimilar geometry is based on the bio-calcite template for the second level, and *bone-like* arrangement at the third level of hierarchy (Fig. 3d inset). Here, the platelets size at the second level of hierarchy is $2.02 \mu\text{m}$ by $0.47 \mu\text{m}$ in cross-section, while at the third level is $12.6 \mu\text{m}$ by $5.5 \mu\text{m}$. Initial crack sizes in these models range from ≈ 5 to $35 \mu\text{m}$. As before, the volume fraction of the two constituents, bulk silica and nanoporous silica, are kept constant at 80% and 20%, respectively, for all cases considered here.

Figure 3a and c shows the stress-strain plot comparing a two-hierarchy *bone-like* structure to a three-hierarchy self-similar assembly. We make two important observations. First, as the hierarchy level is increased we find a decrease in the fracture strength. Second, we observe an increase in defect-tolerance. Figure 3b and d shows the stress-strain plot comparing a two-hierarchy *biocalcitic-like* structure to a three-hierarchy dissimilar structure. In this case, the transition from a two-hierarchy to three-hierarchy system shows only a small change in fracture strength, but as before an increase in the defect-tolerance. An important result from this analysis is a general trend, the observation of an increase in defect-tolerance size scale with the increase in number of hierarchy levels, even though the fracture strength tends to decrease. In Fig. 4 we take a closer look at the origin of the enhanced defect-tolerance. To achieve this we consider several samples of the dissimilar three-hierarchy structure with different crack sizes and identify their fracture strengths (Fig. 4a). We find that despite a 300% increase in crack size from $6 \mu\text{m}$ to $18 \mu\text{m}$ there is only a 24% drop in fracture strength. A detailed analysis of the mechanics of the stress-strain curves is

presented in Figs. 4b and 4c. We observe that the later part of the rising stress region before catastrophic fracture is associated with the opening of a large number of micro-cracks throughout the sample. Once these microcracks start moving and link up to the pre-crack, unstable crack-propagation sets in, leading to a peak in stress and defining the fracture strength. This effect can also be measured through the total new surface area created during the diffuse micro-cracking regime while the main crack does not move (Fig. 4c-d).

To observe whether this pattern of increase in defect-tolerance continues with the number of structural hierarchies, we create a model with four levels of hierarchy, with results shown in Fig. 5. Here, the second structural level is *biocalcitic-like*, while the third and fourth levels are *bone-like* designs. The overall volume fraction of the bulk-silica constituent is maintained at 80% as in all previous models. The overall sample size is $108 \mu\text{m}$ by $140 \mu\text{m}$ in the X - Y plane, and 100 nm in the Z -direction. Figure 5b shows the stress-strain curves for the four-hierarchy structure with various crack sizes from $\approx 6 \mu\text{m}$ to $\approx 64 \mu\text{m}$. Notably, almost no change in fracture strength is observed over this rather large change in the crack size. This finding confirms that the defect-tolerance has improved quite substantially in the four-hierarchy system over that of the two-hierarchy and three-hierarchy structures.

The effect of different hierarchical structures on the fracture properties can be captured effectively through measuring changes in the material crack-propagation resistance curve, the so-called R-curve. The R-curve measures the resistance to fracture $G(\Delta a)$ for a given amount of crack advance length, Δa (details on the calculation of the fracture resistance using the J-integral are given in the Methods section). Figure 5c depicts R-curves for bulk silica and two, three and four hierarchy level structures. We observe a distinct effect of the addition of hierarchies on the R-curve behavior of the material,

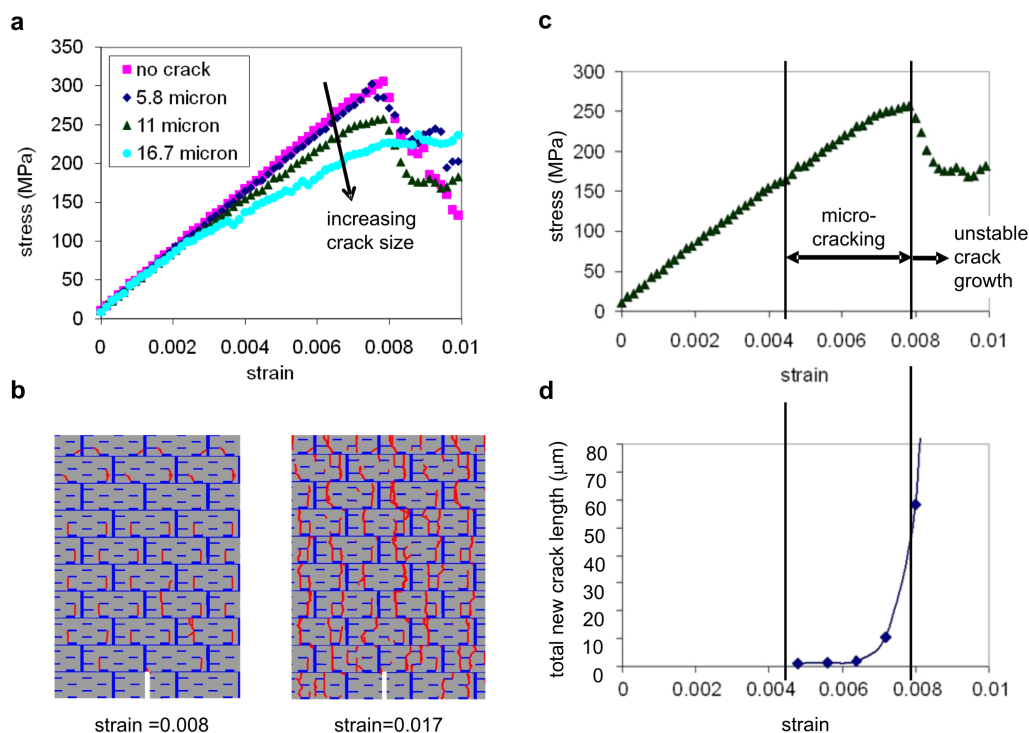


Figure 4 | Detailed analysis of the source of defect tolerance in three-hierarchy structures. a, Stress-strain behavior and fracture strengths for several samples of the dissimilar three-hierarchy structure with different crack sizes. We find that with a 300% increase in crack size from $6 \mu\text{m}$ to $18 \mu\text{m}$ there is only a 24% drop in fracture strength. b and c, The latter part of the rising stress regime before fracture occurs involves the opening of many micro-cracks throughout the sample (crack size $11 \mu\text{m}$). These micro-cracks are shown in red color in panel b, with the numbers indicating applied strain values. Once these microcracks start moving and link up to the pre-crack, there is unstable crack-propagation leading to a drop in stress and thus, the fracture strength. Panel d shows that this effect can also be measured through the total new surface area created during the diffuse micro-cracking regime, during which time the main crack remains stationary. Data shown in panels b–c for the case of a pre-crack length of $11 \mu\text{m}$.



where both the absolute values of G versus crack advance as well as the slope of the R-curve, $\partial G/\partial \Delta a$, increase with the number of hierarchies. The slope of the R-curve has a close relation to the concept of defect-tolerance. As seen in Fig. 6a, in a material with a rising R-curve, unstable crack advance and thus catastrophic failure occurs when the following conditions are satisfied:

$$G_{\text{app}} \geq G_{Ic} \text{ (initiation of stable cracking), and} \quad (1a)$$

$$G_{\text{app}} \geq G \text{ and } \frac{\partial G_{\text{app}}}{\partial \Delta a} \geq \frac{\partial G}{\partial \Delta a} \text{ (initiation of unstable cracking);} \quad (1b)$$

where G_{app} is the applied energy release rate, $G = G(\Delta a)$ is the material fracture toughness from the R-curve, Δa is the advance in the crack length and G_{Ic} is defined as the fracture initiation toughness, where the R-curve intersects $\Delta a = 0$. This, along with the load-to-energy-release relation for an edge crack given by $G_{\text{app}} \sim \sigma^2 \pi a / E$ (where σ and E are the applied stress and elastic modulus, respectively), implies that the load at which a certain crack size a will propagate unstably resulting in catastrophic failure can be directly calculated by marking off the crack size a on the negative X -axis of an R-curve, and constructing the tangent to the R-curve passing through this point, as shown in Fig. 6a. The slope of this curve is proportional to the load or fracture stress at which this crack propagates in an unstable fashion. (And similarly, the slope of the straight line that goes through G_{Ic} is proportional to the load or fracture stress at which this crack starts to propagate in a stable fashion.) Importantly, this also implies that for a rising R-curve, the higher the rate of rise of G with crack advance Δa , the lesser the sensitivity of fracture stress with respect to crack size, and thus the higher the defect-tolerance length scale. Defect-tolerance length scales are thus closely linked to not only the absolute values of fracture-crack

initiation values G_{Ic} ¹⁶ but also to the rising part of the R-curve, and directly visible through the slope of the R-curve. The key finding established in this paper is that these important features can be directly controlled by the incorporation of hierarchical structures, without the need to introduce new materials or any additional mechanisms such as interfacial processes.

Indeed, this theoretical concept is confirmed through our own computational results shown in Figs. 6b and 6c. Here, the fracture stress is measured for two-, three-, and four-hierarchy structures for different crack sizes. The loss of strength as a percentage of the strength of the no-cracked samples has been plotted in Fig. 6b for all the levels of hierarchy. We observe that the sensitivity of fracture strength to crack size drops significantly with increasing hierarchy levels. Assuming that a 10% loss in fracture strength defines the defect-tolerance length scale, Fig. 6c confirms that this length scale increases non-linearly with the number of hierarchies and shows a strong exponential rise of the defect tolerance with increasing levels of hierarchies. We emphasize that this result is generic and independent of the specific definition of the defect-tolerance length scale.

Discussion

The most important result of our study is the demonstration of a design paradigm that explains how materials with superior mechanical properties can be obtained despite the use of a single and structurally “poor” (*i.e.* brittle) base material, realized solely through the use of hierarchical structures without any additional mechanisms such as interfacial effects. Our findings may explain why biological materials universally show hierarchical structures, establishing that they provide a path to turn weakness into strength, and thereby a strategy for an organism’s survival despite the availability of poor construction materials. We achieved this by examining the fracture

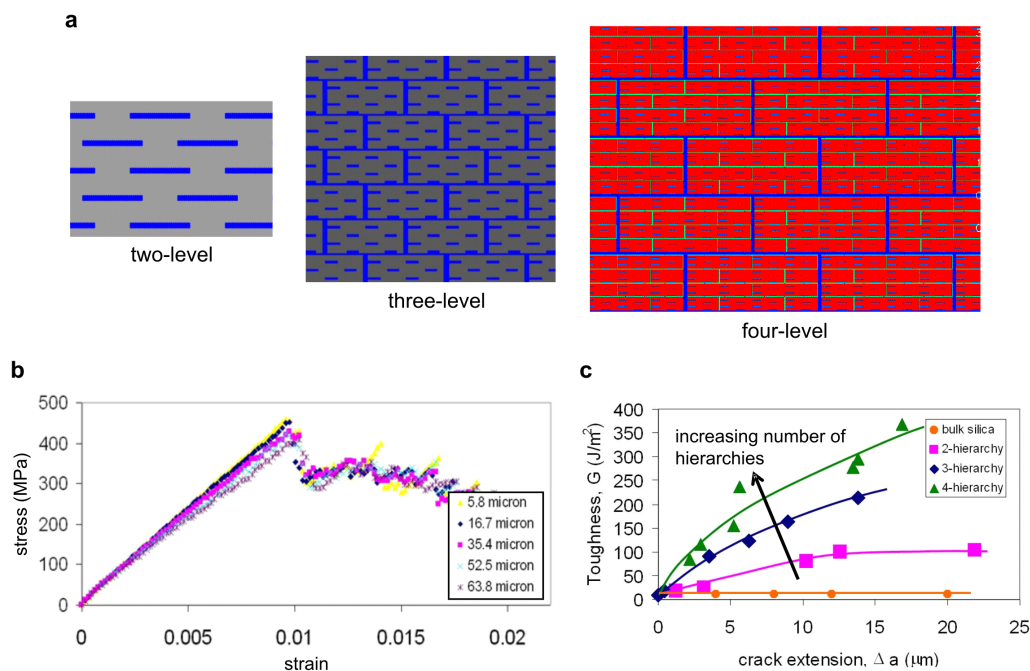


Figure 5 | Geometry of the four-hierarchy level material, stress-strain plots, and R-curve behavior. a, Geometry of two-hierarchy, three-hierarchy and four-hierarchy structures for comparison, with the four-hierarchy structure having a second hierarchical level that is *biocalcite-like*, while the third and fourth levels are *bone-like*. In the four-hierarchy structure, the color scheme is: bulk silica—red, nanoporous silica—green and blue, to show the four levels more clearly. The overall volume fraction of the bulk-silica constituent is kept constant at 80% in all cases. b, Stress-strain curves for the four-hierarchy structure with various crack sizes from $\approx 6 \mu\text{m}$ to $\approx 64 \mu\text{m}$. Almost no change in fracture strength is seen over this very large change in crack size for the four-level hierarchy material. This directly shows that the defect-tolerance has increased substantially over two-hierarchy and three-hierarchy structures. c, R-curve behavior of bulk silica and for two, three, and four levels of hierarchy structures (for initial crack sizes of 6.96 μm , 6.96 μm , 16.7 μm , and 63.8 μm , respectively). The R-curve measures changes in fracture toughness as a crack propagates through the change in energy released per unit length of stable crack advance.



mechanics of hierarchical structures with up to four levels of hierarchy, using an atomistically-informed *in silico* mesoscale model that provided direct access to the fracture mechanics of hierarchical materials. Through a series of simple computational experiments we demonstrated that the defect-tolerance length scale directly increases with number of hierarchy length scales (Figs. 3–5), quickly reaching $\approx 60 \mu\text{m}$ for four levels of hierarchy (Fig. 6); presenting a significant departure by several orders of magnitude from the defect-tolerance length scale of the base material silica alone, which is on the order of a few nanometers. The paradigm illustrated here facilitates the construction of materials that feature stable crack advance for a very large range of crack sizes, and without catastrophic material breakdown.

Notably, stable crack advance is not catastrophic or disabling for biological materials, since materials such as bone have the ability to self-heal over time from fracture³⁹ or from fatigue-induced damage^{40,41}. This agrees directly with our finding that hierarchical materials feature a rising R-curve behavior, across several micrometers and larger length scales, which promotes stable crack advance in the material even if it is subjected to large loads and allows it to be useful beyond its fracture initiation load point. Large loads are dissipated in multiple-hierarchy materials through the initiation and arrest of cracks that occur at different length scales (see Figs. 2d, 4b and 4c). This is in contrast to single hierarchy materials that would shatter with a single crack propagating through the material. If the load does not increase to levels that would lead to unstable crack propagation, this mechanism provides a tissue or an organism the necessary time to repair the material in order to restore its full load

carrying capacity. Our data confirms that a higher number of hierarchies provide an improved rising R-curve behavior despite no additional material used or new mechanisms introduced.

Future work could be aimed at optimizing the R-curve behavior over several micrometers or higher length-scale of crack advance. Both the number of hierarchies, and the design of the geometry of individual hierarchy levels, would have different effects on the entire R-curve shape. Our mesoscale model presents an effective tool that can be utilized for systematic design optimization to maximize R-curve magnitudes and R-curve slope improvements. The model could also be extended to larger length scales, potentially sub-mm, such that R-curve toughness improvements can be seen over length scales that approach macroscopic sample sizes. Further work could also be focused on an improved modeling of the interfaces between soft/hard phases at each hierarchy level, for example to include a specific constitutive behavior. This would enable one to capture the contributions of the interfaces to the toughness at various levels and open additional avenues to improve the material performance. However, it is emphasized here that the model used in this article was chosen deliberately to preclude any additional mechanisms at interfaces to provide a clean model that examines effects solely due to hierarchical structures. Despite the mechanistic insight developed here, the model used in this study is qualitative in nature and the toughness values predicted have to be carefully validated against experimental data. Nevertheless, our results show a manifold increase of key fracture parameters which should hold regardless of the details of the model used.

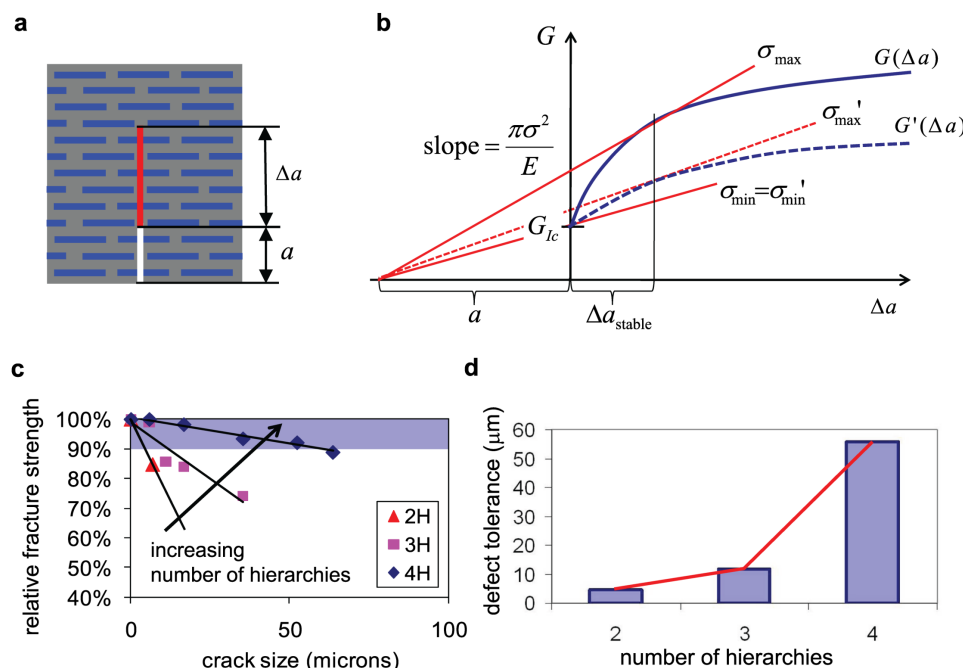


Figure 6 | Relation between the R-curve, rate of fracture strength change with crack size, and the defect-tolerance length scale for varied number of hierarchies. a, Definition of variables a (initial crack length) and Δa (crack advance length). b, Schematic of R-curve $G(\Delta a)$ in a material with a rising R-curve resistance and link to unstable crack propagation. The rising R-curve shown here resembles those seen in hierarchical structures (e.g.: Fig. 5a). The load at which a crack with a certain size will propagate unstably and thus cause catastrophic failure can be calculated by marking off the crack size on the negative- X axis and constructing the tangent to the R-curve passing through this point. The slope of this curve is proportional to the load or fracture stress at which this crack propagates unstably. For comparison the plot also shows a second R-curve ($G'(\Delta a)$) that does not rise as rapidly, resembling those R-curves seen in Fig. 5a for fewer levels of hierarchies. The fracture stress at which the crack propagates unstably is much smaller, indicating a smaller defect tolerance. b, Fracture stress as a percentage loss from the strength of structures with no cracks, measured for two-, three-, and four-hierarchy structures and for varied crack sizes. The shaded region shows the crack sizes with less than 10% loss in strength. The data shows that the sensitivity of the fracture strength to crack size decreases substantially with increasing hierarchy level. c, Plot of the defect-tolerant length scale over the number of hierarchies. The defect-tolerant length-scale reaches $\approx 60 \mu\text{m}$ with four levels of hierarchy. The red line represents an exponential fit of $L = 1.17 \exp(1.255N)$, where L is the defect-tolerant length scale in micrometers, and N is the number of hierarchy levels. The limiting value of one level of hierarchy, *i.e.*, bulk silica, features a vanishing defect-tolerant response on the order of nanometers.



Methods

We use a multiscale bottom-up computational methodology to study the effect of hierarchical design on material properties. At the micron length scale, we use a simple mesoscopic model that describes the material as a collection of particles connected by complex nonlinear springs³⁶, with all parameters informed based on full-atomistic simulations based on reactive force field modeling. The model is designed by our desire to develop a simple model to derive generic insight into the mechanical properties and deformation mechanisms valid for a broader class of hierarchical biological materials. We note that even though such a simple model formulation does not allow us to derive quantitative conclusions for phenomena pertaining to specific types of biological materials, it enables us to understand universal, generic relationships between underlying molecular mechanisms, resulting nonlinear properties of the material, and the failure behavior of hierarchical materials. The level of abstraction used in the present study is critical for our goal to establish fundamental insight into a broader class of materials.

At the nanoscale we use full-atomistic molecular dynamics simulations to study the mechanics of the nanoporous silica structures. We use the first principles based reactive ReaxFF atomistic force field^{42,43}, which effectively captures the energy landscape associated with chemical bond changes, including bond breaking. The ReaxFF description is based on a bond-length bond-order description and fitted to density-functional calculations of energy landscapes of bond-distortion, breaking and forming events. A variety of Si-O clusters were used for fitting parameters, as also energetics of bulk crystalline phases of silicon and silica under tension and compression; all obtained from quantum mechanics calculations (for details see^{42,43}). The ReaxFF potential has been used successfully in predicting fracture phenomena in silicon and silica, and has been validated against experimental data^{33,44,45}. At the micron length scale, with the mesoscale spring-lattice network model, structural loading is carried out by stepped edge displacement boundary conditions and relaxing the global positions of all material particles using a conjugate gradient energy minimization scheme⁴⁶.

The fracture toughness in the mesoscale model is calculated by invoking the J-integral⁴⁷. R-curves are plotted by calculating structure fracture toughness for different values of stable crack advance⁴⁸. Stable crack advance for every load configuration is noted by finding the crack tip location. A particular bond is regarded as broken when its deformation exceeds the cutoff for the interaction. Crack surfaces are visualized by finding all spring bonds which have snapped for a given load. The J-integral is used to find the energy release rate for a given amount of stable crack advance. The plot of the J-integral from the start of crack initiation throughout crack propagation provides the R-curve⁴⁸ for the material, i.e. how its fracture toughness changes as a function of stable crack advance. J-integral calculations for different structures are done with large initial crack sizes. In all cases the initial cracks are chosen large enough to prevent a diffuse micro-cracking response in the entire material, as this would prevent us from carrying out the calculation of the J-integral through the method demonstrated above, due to unavailability of an integration region free of cracks.

A more detailed description of the computational methods is provided in the Supplementary Information section.

- Rho, J. Y., Kuhn-Spearing, L. & Zioupos, P. Mechanical properties and the hierarchical structure of bone. *Medical Engineering & Physics* **20**, 92–102 (1998).
- Sarikaya, M. An introduction to biomimetics: A structural viewpoint. *Microscopy research and technique* **27**, 360–375 (1994).
- Aizenberg, J. *et al.* Skeleton of Euplectella sp.: Structural hierarchy from the nanoscale to the macroscale. *Science* **309**, 275–278 (2005).
- Losic, D., Pillar, R. J., Dilger, T., Mitchell, J. G. & Voelcker, N. H. Atomic force microscopy (AFM) characterisation of the porous silica nanostructure of two centric diatoms. *Journal of Porous Materials* **14**, 61–69 (2007).
- Thiel, B. L., Guess, K. B. & Viney, C. Non-periodic lattice crystals in the hierarchical microstructure of spider (major ampullate) silk. *Biopolymers* **41**, 703–719 (1997).
- Keten, S., Xu, Z., Ihle, B. & Buehler, M. J. Nanoconfinement controls stiffness, strength and mechanical toughness of -sheet crystals in silk. *Nature Materials* **9**, 359–367 (2010).
- Zhang, K., Duan, H., Karihaloo, B. L. & Wang, J. Hierarchical, multilayered cell walls reinforced by recycled silk cocoons enhance the structural integrity of honeybee combs. *Proc Natl Acad Sci U S A* **107**, 9502–6 (2010).
- Kamat, S., Su, X., Ballarini, R. & Heuer, A. H. Structural basis for the fracture toughness of the shell of the conch *Strombus gigas*. *Nature* **405**, 1036–1040 (2000).
- Fratzl, P. & Weinkamer, R. Nature's hierarchical materials. *Progress in Materials Science* **52**, 1263–1334 (2007).
- Launey, M. E., Buehler, M. J. & Ritchie, R. O. On the mechanistic origins of toughness in bone. *Annual Review of Materials Research* **40**, 25–53 (2010).
- Woesz, A. *et al.* Micromechanical properties of biological silica in skeletons of deep-sea sponges. *Journal of Materials Research* **21**, 2068–2078 (2006).
- Nalla, R. K., Kruzic, J. J., Kinney, J. H. & Ritchie, R. O. Mechanistic aspects of fracture and R-curve behavior in human cortical bone. *Biomaterials* **26**, 217–231 (2005).
- Gao, H., Ji, B., Jäger, I. L., Arzt, E. & Fratzl, P. Materials become insensitive to flaws at nanoscale: lessons from nature. *Proceedings of the National Academy of Sciences of the United States of America* **100**, 5597 (2003).
- Gao, H. J. Application of fracture mechanics concepts to hierarchical biomechanics of bone and bone-like materials. *International Journal Of Fracture* **138**, 101–137 (2006).
- Lakes, R. Materials with structural hierarchy. *Nature* **361**, 511–515 (1993).
- Gao, H. Application of fracture mechanics concepts to hierarchical biomechanics of bone and bone-like materials. In: *Advances in Fracture Research* (Springer, New York, 2006), 101–137 (2006).
- Carpinteri, A. & Pugno, N. M. Mechanics of hierarchical materials. *International Journal of Fracture* **150**, 221–226 (2008).
- Bechtle, S., Ang, S. F. & Schneider, G. A. On the mechanical properties of hierarchically structured biological materials. *Biomaterials* (2010).
- Yao, H. & Gao, H. Mechanics of robust and releasable adhesion in biology: bottom-up designed hierarchical structures of gecko. *Journal of the Mechanics and Physics of Solids* **54**, 1120–1146 (2006).
- Yao, H. & Gao, H. Multi-scale cohesive laws in hierarchical materials. *International Journal of Solids and Structures* **44**, 8177–8193 (2007).
- Ritchie, R. O., Buehler, M. J. & Hansma, P. K. Plasticity and toughness in bone. *Phys. Today* **62**, 41–47 (2009).
- Espinosa, H. D., Rim, J. E., Barthelat, F. & Buehler, M. J. Merger of structure and material in nacre and bone-Perspectives on de novo biomimetic materials. *Progress in Materials Science* **54**, 1059–1100 (2009).
- Ackbarow, T. & Buehler, M. J. Alpha-helical protein domains unify strength and robustness through hierarchical nanostructures. *Nanotechnology* **20**, 075103 (2009).
- Zhao, Q., Cranford, S., Ackbarow, T. & Buehler, M. J. Robustness-strength propagation of hierarchical alpha-helical protein filaments. *International Journal of Applied Mechanics* **1**, 85–112 (2009).
- Ackbarow, T. & Buehler, M. J. Hierarchical Coexistence of Universality and Diversity Controls Robustness and Multi-Functionality in Protein Materials. *Journal Of Computational And Theoretical Nanoscience* **5**, 1193–1204 (2008).
- Buehler, M. J. Strength in numbers. *Nat. Nanotechnol* **5**, 172–174 (2010).
- Buehler, M. J. Tu (r) ning weakness to strength. *Nano Today* **5**, 379–383 (2010).
- Griffith, A. A. The phenomena of rupture and flow in solids. *Philosophical transactions of the royal society of london. Series A, containing papers of a mathematical or physical character* **221**, 163–198 (1921).
- Kanninen, M. F. & Popelar, C. L. *Advanced Fracture Mechanics* (Oxford University Press, New York, 1985).
- Bazant, Z. *Scaling of Structural Strength* (Hermes Penton Science, London, 2002).
- Hamm, C. E. *et al.* Architecture and material properties of diatom shells provide effective mechanical protection. *Nature* **421**, 841–3 (2003).
- García, A. P. & Buehler, M. J. Bioinspired nanoporous silicon provides great toughness at great deformability. *Computational Materials Science* **48**, 303–309 (2010).
- García, A. P., Sen, D. & Buehler, M. J. Hierarchical silica nanostructures inspired by diatom algae yield superior deformability, toughness and strength. *Metallurgical and Materials Transactions A*, doi: 10.1007/s11661-010-0477-y (2011).
- Sen, D., García, A. P. & Buehler, M. J. Mechanics of nano-honeycomb silica structures: A size-dependent brittle-to-ductile transition. *Journal of Nanomechanics and Micromechanics* (2011).
- Ostlund, F. *et al.* Brittle-to-Ductile Transition in Uniaxial Compression of Silicon Pillars at Room Temperature. *Advanced Functional Materials* **19**, 2439–2444 (2009).
- Sen, D. & Buehler, M. J. Atomistically-informed mesoscale model of deformation and failure of bioinspired hierarchical silica nanocomposites. *International Journal of Applied Mechanics* **2**, 699–717 (2010).
- Berman, A. *et al.* Intercalation of sea urchin proteins in calcite: study of a crystalline composite material. *Science* **250**, 664 (1990).
- Aizenberg, J. Nanomechanics of Biological Single Crystals. *Nanomechanics of Materials and Structures*, 99–108 (2006).
- Brighton, C. T. & Hunt, R. M. Early histological and ultrastructural changes in medullary fracture callus. *The Journal of Bone and Joint Surgery* **73**, 832 (1991).
- Burr, D. B., Martin, R. B., Schaffler, M. B. & Radin, E. L. Bone remodeling in response to in vivo fatigue microdamage. *Journal of Biomechanics* **18**, 189–200 (1985).
- Verborgt, O., Gibson, G. J. & Schaffler, M. B. Loss of osteocyte integrity in association with microdamage and bone remodeling after fatigue in vivo. *Journal of Bone and Mineral Research* **15**, 60–67 (2000).
- Van Duin, A. C. T., Dasgupta, S., Lorant, F. & Goddard III, W. A. ReaxFF: a reactive force field for hydrocarbons. *J. Phys. Chem. A* **105**, 9396–9409 (2001).
- Van Duin, A. C. T. *et al.* ReaxFFSiO reactive force field for silicon and silicon oxide systems. *J. Phys. Chem. A* **107**, 3803–3811 (2003).
- Buehler, M. J., Tang, H., van Duin, A. C. T. & Goddard III, W. A. Threshold crack speed controls dynamical fracture of silicon single crystals. *Physical Review Letters* **99**, 165502 (2007).
- Sen, D., Thaulow, C., Schieffer, S. V., Cohen, A. & Buehler, M. J. Atomistic Study of Crack-Tip Cleavage to Dislocation Emission Transition in Silicon Single Crystals. *Physical Review Letters* **104**, 235502 (2010).
- Polyak, B. T. The conjugate gradient method in extremal problems* 1. *USSR Computational Mathematics and Mathematical Physics* **9**, 94–112 (1969).
- Rice, J. R. A path independent integral and the approximate analysis of strain concentration by notches and cracks. *Journal of applied mechanics* **35**, 379–386 (1968).



48. Bencher, C. D., Sakaida, A., Rao, K. T. V. & Ritchie, R. O. Toughening mechanisms in ductile niobium-reinforced niobium aluminide (Nb/Nb₃Al) in situ composites. *Metallurgical and Materials Transactions A* **26**, 2027–2033 (1995).
49. Kroger, N. Prescribing diatom morphology: toward genetic engineering of biological nanomaterials. *Current Opinion in Chemical Biology* **11**, 662–669 (2007).

Acknowledgements

This work was supported by the Army Research Office (DOD). The authors acknowledge helpful discussions with L. Gibson, C. Schuh and S. Allen (MIT).

Author contributions

M.B. and D.S. designed the research and analyzed the results. D.S. carried out simulations and data analysis. M.B. and D.S. wrote the paper.

Additional information

Supplementary Information accompanies this paper at <http://www.nature.com/scientificreports>

Competing financial interests: The authors declare no competing financial interests.

License: This work is licensed under a Creative Commons Attribution-NonCommercial-NoDerivative Works 3.0 Unported License. To view a copy of this license, visit <http://creativecommons.org/licenses/by-nc-nd/3.0/>

How to cite this article: Sen, D. & Buehler, M.J. Structural hierarchies define toughness and defect-tolerance despite simple and mechanically inferior brittle building blocks. *Sci. Rep.* **1**, 35; DOI:10.1038/srep00035 (2011).